

Wintertime Evolution of the Temperature Inversion in the Colorado Plateau Basin

C. DAVID WHITEMAN, XINDI BIAN, AND SHIYUAN ZHONG

Pacific Northwest National Laboratory, Richland, Washington

(Manuscript received 14 April 1998, in final form 15 June 1998)

ABSTRACT

The Colorado Plateau, surrounded by a ring of mountains, has the meteorological characteristics of a basin. Deep, persistent potential temperature inversions form in this basin in winter. The formation, maintenance, and dissipation of these inversions are investigated using two to four times daily radiosonde data from the winter and early spring of 1989–90. In winter, inversion evolution is forced primarily by synoptic-scale events. The buildup takes place over one or more days as warm air advection occurs above the basin with the approach of high pressure ridges. The breakup, which occurs with cold air advection above the basin as troughs approach, can occur over periods less than 12 h. Many approaching troughs modulate inversion strength and depth but are too weak to destroy the persistent inversion. Later in the winter and spring, the radiation-induced nocturnal inversion is destroyed nearly every day by the daytime growth of convective boundary layers from the basin floor and sidewalls.

1. Introduction

A recent panel (Smith et al. 1997) considered research needs and opportunities in mountain meteorology and called for new observational and numerical modeling research on the development, maintenance, and removal of cold air pools or temperature inversions in basins and valleys. The research was considered a high priority because scattered areas of high population are found in valleys and basins where cold air can be trapped for long periods, producing significant effects on human activities. Air pollution can accumulate to unacceptably high levels in basins (Reddy et al. 1995), and cold air pools can lead to hazardous episodes of persistent freezing rain, drizzle, or fog (Petkovsek 1974). Further, in cold climates, cold air pools lead to delays in thawing of wintertime snow cover, interfering with ground transportation (Smith et al. 1997).

While a significant body of literature now exists on inversion buildup and destruction in valleys (reviewed by Whiteman 1990) little effort has, so far, been expended on improving understanding of cold air pools in basins. Persistent pools occur primarily in winter, but few datasets have been available to investigate this phenomenon. Nonetheless, research on related problems in basins, such as the formation of drainage flows, development of boundary layers, and basin energetics has been conducted throughout the world, with contribu-

tions coming largely from Yugoslavia, Japan, and the United States.

Because the Adriatic coasts of Slovenia and Croatia have large areas of limestone, they have many sinkholes and basins. Air pollution problems in these basins have been widely recognized and studied (e.g., Petkovsek 1978, 1980, 1992; Vrhovec 1991). In wintertime, the basins are often capped by low clouds, which decrease insolation and cause cold air pools to persist for long periods (Petkovsek 1974). Investigations in Japanese basins have focused on basin surface and atmospheric energy budgets (Kondo et al. 1989; Kondo and Okusa 1990; Ishikawa 1977; Kuwagata et al. 1990a, 1990b; Kuwagata and Sumioka 1991). In addition, numerical simulations of thermally driven circulations have been performed with the goal of understanding pollutant transport from Tokyo and other industrial areas into nearby basins (Kimura and Kuwagata 1993). In the United States, meteorological research has been conducted in basins ranging in size from 10^2 to 10^5 km², including Colorado's Sinbad (Fast et al. 1996; Whiteman et al. 1996) and South Park (Banta 1984) Basins, Virginia's Roanoke Basin (Allwine et al. 1992), the Columbia Basin (Staley 1959; Doran and Zhong 1994), the Los Angeles Basin (Smith et al. 1980; Glendening 1990; Ulrickson and Mass 1990; Lu and Turco 1995, 1996), and the Great Basin (Wolyn and McKee 1989; Mayr and McKee 1995; Savoie and McKee 1995).

This paper investigates the wintertime formation, maintenance, and dissipation of cold air pools over the Colorado Plateau using data from the 1989–90 Navajo Generating Station Winter Visibility Study (WVS). The

Corresponding author address: Dr. C. David Whiteman, K9-30, Battelle Northwest Laboratories, P.O. Box 999, Richland, WA 99352.
E-mail: Dave.Whiteman@pnl.gov

Colorado Plateau, surrounded by mountains, has the topographical characteristics of a large basin and will be referred to in this paper as the Colorado Plateau Basin. The data were collected as part of a program to investigate the sources of visibility degradation in Grand Canyon National Park and the meteorological mechanisms leading to low-visibility episodes (Richards et al. 1991; Lindsey et al. 1999). The experiments were performed over a period of about 3 months and included measurements from radar wind profilers, upper-air sounding devices, and a surface tower network. Other analyses using these data have focused on Grand Canyon meteorology (Banta et al. 1999; Whiteman et al. 1999a), on surface wind patterns (Whiteman et al. 1999b; Kaufmann and Whiteman 1999), and on air pollution dispersion (Allwine and Whiteman 1994; Lindsey et al. 1999; Chen et al. 1999).

The Colorado Plateau Basin area is well known for its wintertime inversions. Radiosonde summaries from the National Weather Service site at Winslow, Arizona, at the south end of the basin, indicate that surface-based temperature inversions deeper than 250 m are present more than 50% of the time in winter 1200 UTC (0400 MST) soundings (Holzworth 1972; Holzworth and Fisher 1979). This is the highest frequency of such inversions among radiosonde stations in the contiguous United States. Morning inversions exceed 500 m in depth nearly 36% of the time in winter. Winslow also has an unusually high frequency of elevated inversions in winter afternoon radiosonde soundings, and mean winter morning mixing heights are the lowest in the contiguous United States.

The goals of this study were to determine the characteristics of the wintertime inversions in the Colorado Plateau Basin, to investigate the physical processes responsible for their formation, maintenance, and destruction, and to determine how the inversion characteristics and processes change through the course of the winter and early spring. The study finds that the inversion evolution cycle is driven primarily by synoptic-scale weather events in midwinter, but becomes more and more influenced by diurnal radiation-induced boundary layer processes inside the basin by late winter and early spring.

The following section describes the basin topography, the data collection sites, and the data. Section 3 describes the horizontal structure of the inversion over the Colorado Plateau Basin, while section 4 presents the bulk characteristics of the basin temperature inversion at the morning and afternoon sounding times and their variation with time during the 80-day experimental period. Section 5 then looks at the time series of potential temperatures at the floor and top of the basin as a means of diagnosing inversion structure evolution. In section 6, an alternative means of diagnosing inversion evolution is developed by computing heat storage in the basin atmosphere. Changes in basin heat storage during the experimental period are then related to synoptic-

scale and basin-scale meteorological variables to evaluate mechanisms that lead to inversion buildup, maintenance, and breakup. This is followed by a discussion in section 7 and a summary and conclusions in section 8.

2. Topography, observing sites, and data

The Colorado Plateau, one of the major geological provinces of North America (Harris 1978) covers an area of about 225 000 km² in western Colorado, northwestern New Mexico, eastern Utah, and northern Arizona (Fig. 1). The semiarid area consists of a complex mixture of mesas, plateaus, and canyons that are surrounded by a rim of high mountains. The Colorado River flows through this basin from northeast to southwest and receives a number of tributaries coming from the Rocky Mountains to the north and east. The southern and western edges of the plateau adjoin the sprawling Basin and Range Province, which extends south from Oregon to Mexico and eastward to southwestern Texas and is characterized by a large number of short, mostly north-south-oriented mountain ranges that are separated by wide basins. The Grand Canyon is the major channel connecting the two provinces.

The locations of selected WVS upper-air sounding sites are shown in Fig. 1. Further information on the sites, including measurement types and frequencies, is provided in Table 1. Except for Ash Fork (ASH), which is located west of the plateau in the Basin and Range Province at 1588 m MSL, all other WVS sites were located within the Colorado Plateau Basin. Among them, four were low-elevation sites [1000–1350 m above mean sea level (MSL)] located at the Colorado [Dangling Rope (DNG), Bullfrog Basin (BUL), Page (PGA)] and Little Colorado [Cameron (CAM)] Rivers, and one [Tusayan (TUS)] was a high-elevation site (2012 m MSL) located on the Coconino Plateau on the southwestern boundary of the basin.

The upper-air sounding portion of the WVS was conducted from 10 January through 31 March 1990. This winter period was a typical winter in terms of the number of low-visibility episodes and the general weather conditions, except that the region was influenced by more closed lows than in a normal winter and that southwesterlies were somewhat more frequent in the basin than in a normal winter (Richards et al. 1991). At most of the sites, radiosondes were launched twice per day at 0400 and 1600 MST during this period, except during Intensive Observational Periods (IOPs) when sondes were launched at 0400, 1000, 1600, and 2200 MST to support special chemical and aircraft experiments. Because this sounding frequency is relatively low, the data are not suitable for investigating rapid evolutionary changes in cold pool characteristics such as might occur with diurnal buildup and breakup of the cold pool. Thus, this paper focuses primarily on the bulk characteristics of the basin cold pool at 12-hourly intervals.

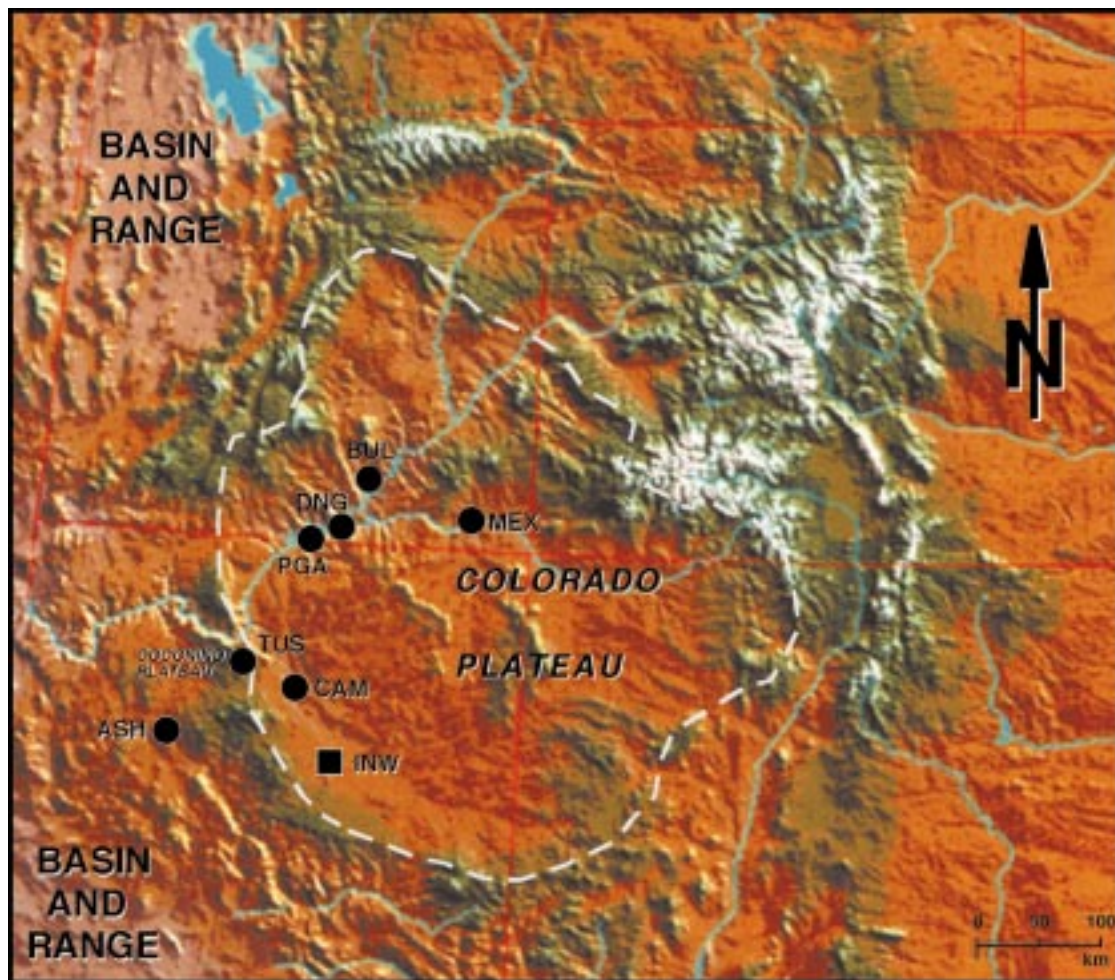


FIG. 1. Locations of selected WVS upper-air sounding sites (dots) in the Grand Canyon region. The National Weather Service radiosonde station at Winslow is also shown (square), along with major topographical features.

3. Spatial variations of boundary layer structure over the Colorado Plateau basin

Spatial variations in vertical potential temperature structure on clear undisturbed days with weak winds aloft, as seen from six WVS basin sites on 11 and 12 January 1990, are presented in Figs. 2 and 3, respec-

tively. On these days, a particularly strong inversion was present in the basin, but inversion characteristics differed among the basin sites in a way that is typical for this region.

The 1600 MST soundings on 11 January (Fig. 2) show that the elevated remnant of a nocturnal inversion was present within the basin with a relatively level top

TABLE 1. Selected site names, abbreviations, locations, instrumentation, and observation frequencies.

Site name	Site ID	Latitude (°N)	Longitude (°W)	Elevation (m MSL)	Sounding type*
Ash Fork, AZ	ASH	35°14'21"	112°29'00"	1588	RS 2/2
Bullfrog Basin, UT	BUL	37°31'08"	110°43'30"	1130	RS 2/4
Cameron, AZ	CAM	35°50'54"	111°25'39"	1350	RS 0/4
Dangling Rope, UT	DNG	37°07'48"	111°04'53"	1155	RS 0/4
Mexican Hat, AZ	MEX	37°08'56"	109°51'42"	1271	none
Page, AZ	PGA	36°54'47"	111°28'45"	1332	RP, AS 2/4
Tusayan, AZ	TUS	35°57'	112°09'	2012	RS 2/4
Winslow, AZ	INW	35°01'	110°44'	1488	RS 2/2

* RS: radiosonde, RP: radar profiler, AS: optically tracked airsonde. "2/4" indicates 2 soundings per day, increasing to 4 per day during intensive observation periods.

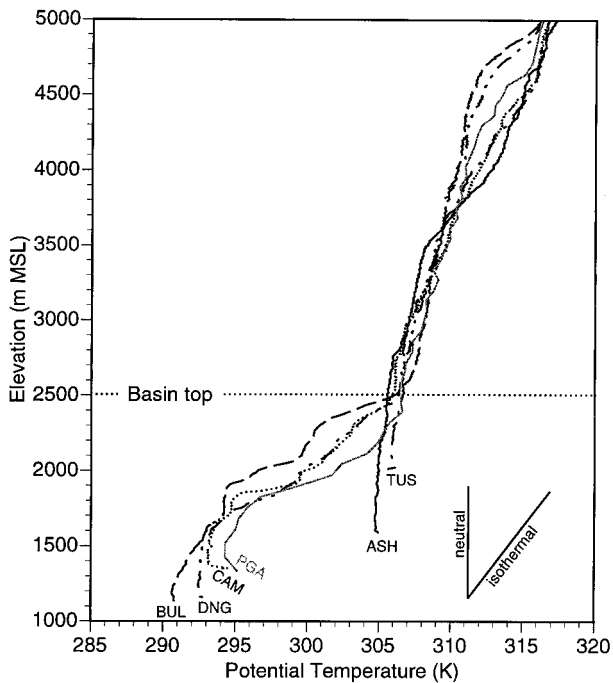


FIG. 2. Potential temperature soundings at six WVS sites at 1600 MST, 11 January 1990. The dotted line is the elevation at the top of the basin. Potential temperature gradients corresponding to neutral and isothermal stabilities are shown for comparison.

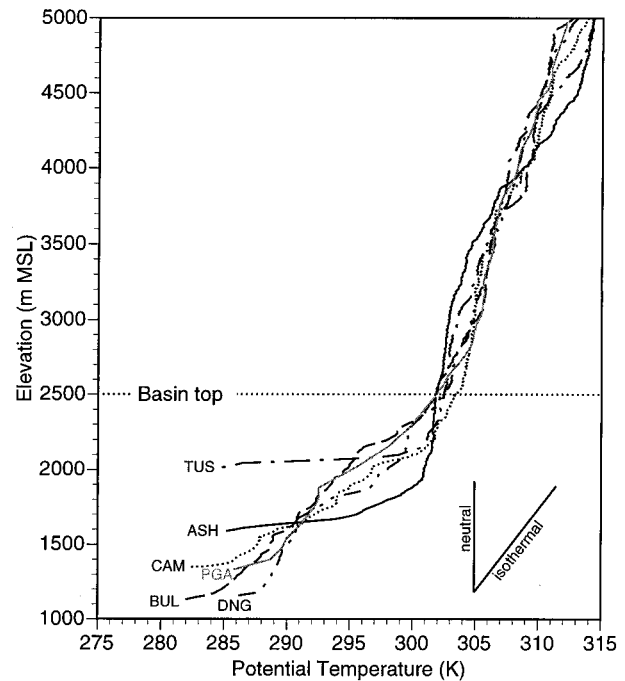


FIG. 3. Potential temperature soundings at six WVS sites at 0400 MST, 12 January 1990. The dotted line is the elevation at the top of the basin. Potential temperature gradients corresponding to neutral and isothermal stabilities are shown for comparison.

at 2500 m MSL. At each of the sounding sites, convective boundary layers (CBLs) had grown upward from the basin surface into the base of this inversion. The daytime CBL had broken the inversion above the high-elevation Tusayan and Ash Fork sites but had failed to destroy the basin inversion above the four low-elevation sites. This failure to break the inversion is caused by the relatively low wintertime surface sensible heat fluxes in the basin. The persistent basin inversion shields the basin from the stronger winds that flow over the basin at levels above the surrounding mountains, and allows multiday stagnation episodes to occur within the basin. CBL depths at the four basin floor sites were variable (~ 200 – 500 m), and winds within the CBL tended to blow up the local slopes in the vicinity of the stations (see Whiteman et al. 1999b). The vertical potential temperature gradient above the CBLs but within the basin inversion was similar at all the sites, but substantial horizontal potential temperature gradients were present between sites.

The 0400 MST soundings on 12 January (Fig. 3) show that a surface-based potential temperature inversion was present above all the basin sites. The vertical potential temperature gradients in the upper two-thirds of the inversion varied little from site to site, and the altitude of the inversion top was generally uniform across the basin (2200–2500 m MSL, except at Page where it was 2800 m MSL). These inversion top heights are roughly equivalent to the mountain heights on the

western edge of the basin. The consistency in inversion top height and potential temperature gradient in the upper part of the inversion from site to site, as seen also in the afternoon soundings, indicates that the inversion or cold pool is a large-scale feature that extends over the entire Colorado Plateau Basin. Differences in basin inversion characteristics at the lowest altitudes of the basin are caused by local topographic and surface energy budget variations in subbasins. Since the basin inversion top is at a near-constant MSL height, the above-ground-level (AGL) heights of the basin inversion top vary from station to station depending on station altitude. Shallow, intensely stable sublayers form immediately above the ground at stations on the floor and sidewalls of the basin as downward sensible heat flux removes heat from the overlying air to counter the long-wave loss of radiation from the surface at night. Down-slope winds are produced in these shallow inclined boundary layers (Whiteman et al. 1999b). At Ash Fork, located outside the Colorado Plateau Basin in the Basin and Range Province, an inversion was also present. Its characteristics differed from those of the Colorado Plateau Basin inversion seen at the other sites. It extended only to 1900 m MSL, rather than 2500 m MSL, and is believed to represent the top of the inversion in the Basin and Range Province west of the Colorado Plateau. The inversion at Ash Fork exhibited a shallow intensely stable sublayer like that at the high-altitude Tusayan station on the basin slope of the Coconino Plateau, a charac-

teristic that is typical of sites on the sloping upper side-walls of basins.

4. Characteristics of the basin inversion and their seasonal variation

The bulk structure of the basin inversion during the 80-day experimental period is illustrated using data from morning and afternoon radiosonde soundings at Bullfrog Basin. This site is chosen for illustration since it is a low-altitude site that is more centrally located than the other radiosonde sites and has a long period of record with good sounding data. Basin inversion and CBL depths were determined from individual soundings by noting the heights of major changes in the slope of the potential temperature profiles. The study focuses on determining the characteristics of inversions within the basin below the altitude of 2500 m MSL, the approximate elevation of the highest topography on the southwestern edge of the basin. This height is 1370 m above Bullfrog Basin.

The nocturnal inversion in the basin, as observed from radiosondes launched at 0400 LST, frequently extended above the basin early in the experimental period (Fig. 4a). In these instances it was often difficult to define the top of the basin inversion as there was no apparent break in stability between the basin and the overlying atmosphere. The inversion top was increasingly found at lower elevations within the basin after the end of February. Morning potential temperature gradients (Fig. 4b), computed from the potential temperature differences between the basin top and the surface (1130 m MSL), averaged 0.0061 ± 0.0033 (standard deviation) K m^{-1} over the entire experimental period, but the potential temperature gradients decreased somewhat between midwinter and spring. Key characteristics of the basin inversion in winter are the considerable day-to-day variability in the morning potential temperature gradients and the propensity for stable layers to extend through the entire basin depth into the atmosphere above.

The afternoon (1600 LST) soundings often exhibited convective boundary layers that had grown upward from the heated floor of the basin during the daytime, but were still capped by the elevated remnants of the nocturnal basin inversion. On some winter days early in the experimental period the atmosphere remained stable all day so that no CBLs were present in the afternoon soundings. On other days, the CBLs extended only part-way through the depth of the basin. The frequency of deep CBLs increased later in the winter and early spring, with many days having CBLs that grew through the entire depth of the basin (Fig. 5a). Afternoon potential temperature gradients, calculated from potential temperature differences between the basin top and the surface, averaged $0.0016 \pm 0.0026 \text{ K m}^{-1}$ over the experimental period. The gradients fell off steeply from midwinter values as spring approached (Fig. 5b).

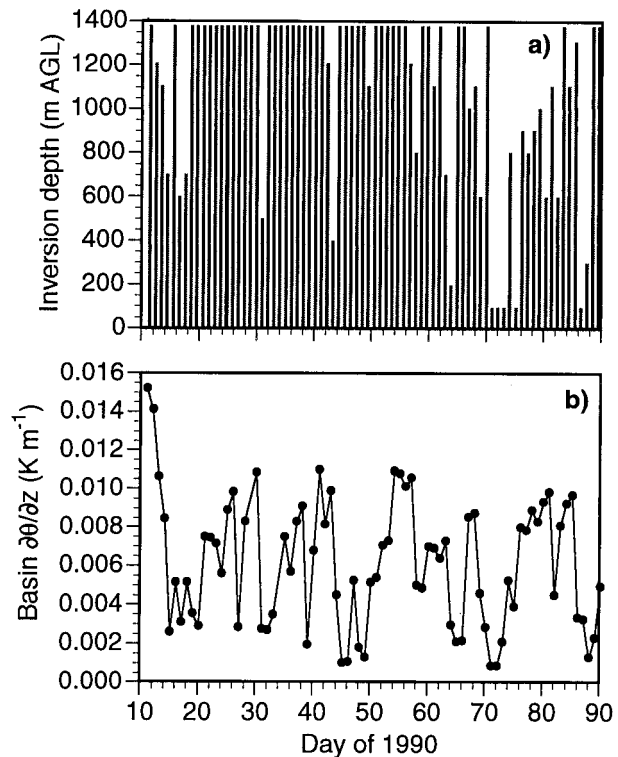


FIG. 4. Bulk characteristics of the basin atmosphere as summarized from the morning (0400 MST) BUL soundings. (a) Inversion depth (depths extending above the basin are set to the basin depth) and (b) potential temperature gradient as calculated over the 1370-m basin depth.

The mean wind structure in the basin is shown in Fig. 6 as a time-height cross section of mean hourly horizontal vector winds and wind persistence (the ratio of vector average and scalar average winds) at Page, Arizona, obtained from averaging the hourly radar wind profiler measurements over the entire experimental period. Radar profilers measure the Doppler-shifted radar returns backscattered from clear-air refractive index inhomogeneities that are advected by the mean wind. Because humidity is often low and turbulence weak in the basin inversion, the vertical range of the Page profiler was limited, so that the figure shows only the 11 layers having approximately 25% or greater data recovery. Mean wind speeds are less than 2 m s^{-1} below 1800 m MSL and less than 4 m s^{-1} below the top of the basin at all hours of the day. Wind speeds are low because the wintertime inversion tends to isolate the basin atmosphere from the prevailing southwesterly winds aloft. Winds within the basin above Page are generally southwesterly during the period of daytime heating, and are westerly or west-southwesterly during the rest of the day. The stronger mean speeds in the upper altitudes of the basin are produced when traveling synoptic-scale storms sweep across the basin in winter and, later in the winter and early spring, when convective boundary layers break the basin inversion on a daily basis. Wind

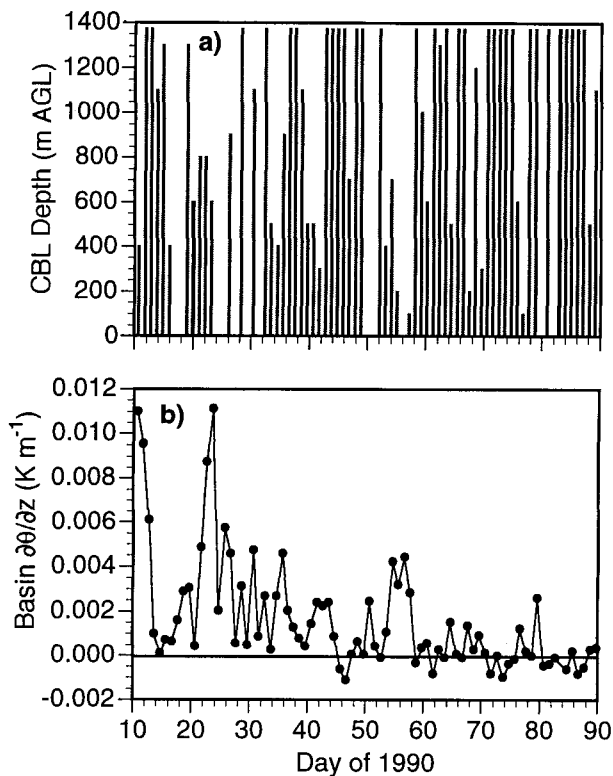


FIG. 5. Bulk characteristics of the basin atmosphere as summarized from the afternoon (1600 MST) BUL soundings. (a) CBL depth (depth \leq basin depth), (b) potential temperature gradient as calculated over the 1370-m basin depth.

persistence (Panofsky and Brier 1965; Whiteman et al. 1999b) is generally low (0.2–0.4) in the basin, except during the afternoon when it reaches 0.5 in the upper half of the basin. Wind persistences and diurnal variability of vector winds are probably somewhat underreported and overreported in the upper levels of Fig. 6, respectively, because of missing data. Analyses of hourly wind data collected from a network of 15 short towers within the basin have shown the important effects of nearby topographic features on surface wind statistics (Sutherland 1992; Whiteman et al. 1999b). The surface winds follow distinctive spatial and diurnal patterns that are related to large-scale synoptic patterns and to time of day (Kaufmann and Whiteman 1999). Stagnation and recirculations at different altitudes in the basin are key features of the wintertime meteorology (Allwine and Whiteman 1994). Inspection of individual wind soundings shows that strong winds from traveling storm systems often penetrate into the upper levels of the basin, but do not often extend to the basin floor.

Individual soundings did not generally show sharp changes in vertical profiles of potential temperature, wind speed, or wind direction at altitudes above Bullfrog Basin corresponding to upwind mountain heights. Southwest winds and north winds must travel about 150 km after crossing the mountains on the edge of the basin

before reaching Bullfrog Basin, while west winds must travel 90 km. Vertical mixing over these travel distances and the varying altitudes of inflows into the basin caused by variations in ridgeline elevations are apparently sufficient to remove any discontinuities in the profiles produced by flows over the basin periphery. Such discontinuities in potential temperature (typically 6 K over 200 m) have been seen, for example, at the top of the Grand Canyon southwest of Bullfrog Basin during periods of strong warm air advection (Whiteman et al. 1999b).

It is interesting to note that inversion characteristics in the Colorado Plateau Basin in wintertime do not support the use of the term “cold air pool.” A cold pool should have a distinctive top that is below the surrounding topography and a temperature deficit relative to the atmosphere above. Because the mean potential temperature gradient within the basin inversion is typically less than that of an isothermal atmosphere ($\partial\theta/\partial z = 0.0098 K m^{-1}$), a true temperature inversion ($\partial T/\partial z > 0$) is often absent, as is a distinctive inversion top.

5. Evolution of potential temperature structure in the basin

The temporal evolution of the basin inversion during the experimental period is summarized in Fig. 7, which shows the surface and basin top potential temperatures at Bullfrog Basin. All radiosonde soundings at this site during the experimental period are plotted in the figure. The gray shading between the two potential temperature time series indicates the presence of a basin potential temperature inversion, with vertical distance between curves providing a measure of inversion strength. The basin inversion is destroyed when the surface potential temperature equals or exceeds the basin top potential temperature.

Several key features of basin inversion evolution are apparent in Fig. 7. First, the basin inversion can persist for many days in midwinter (e.g., days 10–15, 15–20, 20–27), when the diurnal heating at the surface is insufficient to break through the deep and strong basin inversion. After late February, however, the diurnal temperature oscillations at the surface begin to break the inversion on a nearly daily basis. This seasonal change in inversion destruction behavior is caused by seasonal changes in insolation and sensible heat flux in the basin. Daily solar radiation and sensible heat flux increase as the sun gets higher in the sky (less attenuation of the solar beam), the days grow longer, and the desert surface dries (less evaporative energy loss), increasing the Bowen ratio. Daily total solar radiation (Fig. 8) increases by a factor of 2 between the beginning and end of the experimental period. Second, inversion strength and persistence are very much affected by temperature oscillations at the top of the basin produced by passing synoptic-scale weather systems. Large potential temperature oscillations at the top of the basin are seen during the entire experimental period. The period of

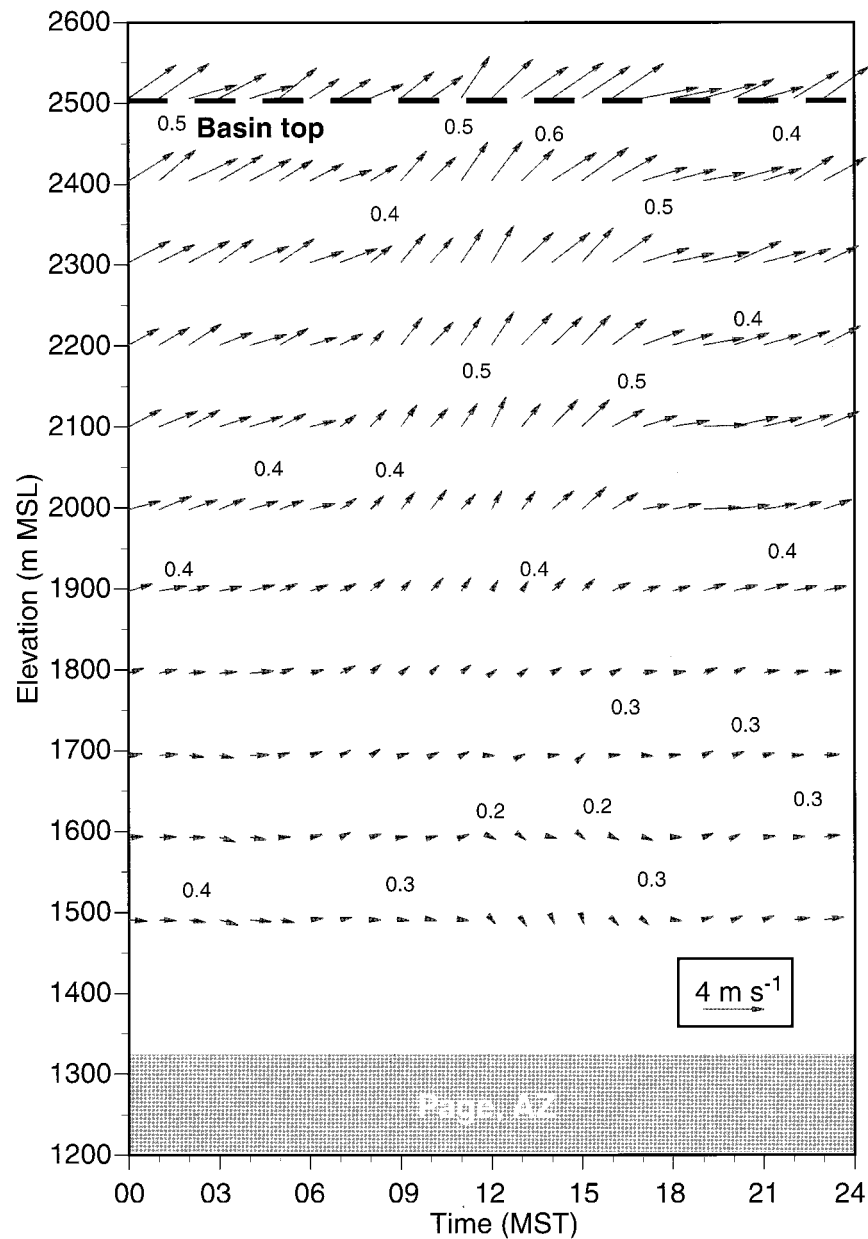


FIG. 6. Time-height cross section of mean horizontal winds as determined from hourly radar profiler wind data at Page, Arizona, over the period from 8 January to 3 April 1990. A vector pointing up represents a wind blowing from south to north, a vector pointing to the right blows from west to east, etc. The dashed line is the elevation at the top of the basin. The labeled solid lines are wind persistence.

these oscillations varies between several days (e.g., the complete cycle from days 24 to 29) and tens of days (e.g., the half-cycle between days 72 and 82). A close inspection of Fig. 7 shows that temperature decreases at the top of the basin leading to inversion breakup tend to occur more rapidly than temperature increases that lead to inversion buildup. Sudden cooling at the basin top led to destruction of the cold pool on days 28, 45, and 70. These episodes of inversion destruction differ

from the daily inversion destruction episodes that occur in the spring in that they are initiated by cooling aloft rather than by diurnal heating inside the basin. Inversion breakups are, nevertheless, assisted by afternoon heating inside the basin. Third, diurnal surface temperature oscillations vary somewhat from day to day depending on cloudiness, but have an amplitude of about 7–10 K on clear days. Diurnal temperature oscillations of this size in the Colorado Plateau Basin lead to a regular daily

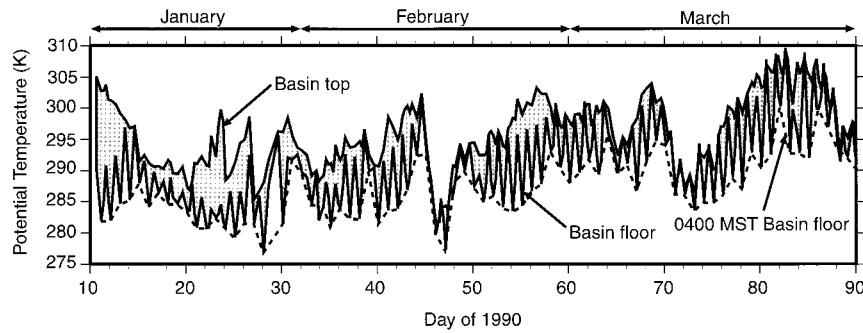


FIG. 7. Time series of surface and basin top (1400 m AGL or 2530 m MSL) potential temperatures at Bullfrog Basin. The upper solid line is the basin top potential temperature, the lower solid line is the surface potential temperature and the dashed line connects the 0400 MST surface potential temperatures. Date labels are plotted at the beginning of the day indicated.

destruction of the inversion after about day 60. Fourth, the surface and basin top potential temperatures, as expected, increase gradually from winter to spring.

The complicated pattern of evolution of the inversion in the Colorado Plateau Basin can be investigated further by considering a set of idealized evolutionary patterns and determining to what extent they (or their combinations) are present in the actual data. An idealized pattern for nonpersistent inversions that are destroyed on a daily basis is shown in Fig. 9. Following this pattern, the surface potential temperature in the afternoon attains or slightly exceeds the basin top potential temperature as an unstable boundary layer grows upward through the basin atmosphere. This pattern becomes increasingly common late in the experimental period (see Fig. 7).

A set of idealized patterns for persistent multiday inversions is shown in Fig. 10. These idealized patterns, as for the daily destruction pattern, are constructed under the assumption that the diurnal surface temperature cycle is regular from day to day. For the persistent cold pools, we also assume that the basin inversion does not exceed ridgetop height. The idealized patterns could be

easily modified to relax these assumptions. The first set of three patterns (Figs. 10a–c) depicts multiday episodes in which potential temperature is constant at the basin top. In (a), the daytime gain in heat storage within the basin balances the nighttime loss so that the inversion maintains its strength over a series of days. Day/night imbalances in heat storage gains and losses in the basin can result in (b) an increase or (c) a decrease in inversion strength over a multiday period. In early winter, nighttime atmospheric losses of sensible heat are expected to be greater than daytime gains, so that the basin inversion would strengthen over a series of days. The assumption of constant basin top potential temperature in this simple pattern is clearly a poor approximation to the actual data in Fig. 7. There are, however, sequences of days in which minimum temperatures at the basin floor increase steadily from day to day (e.g., days

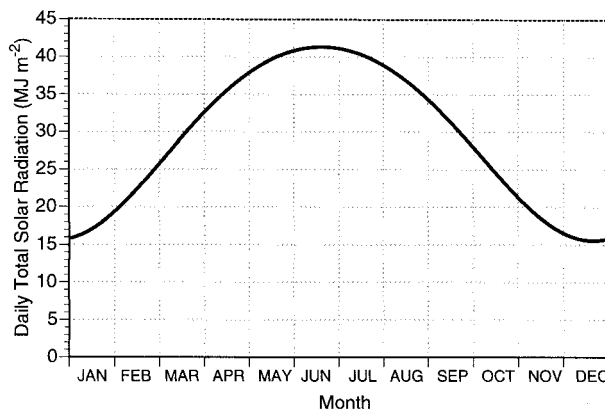


FIG. 8. Daily total extraterrestrial solar radiation as a function of day of year at a latitude corresponding to the center of the Colorado Plateau. From Whiteman and Allwine's (1986) solar model.

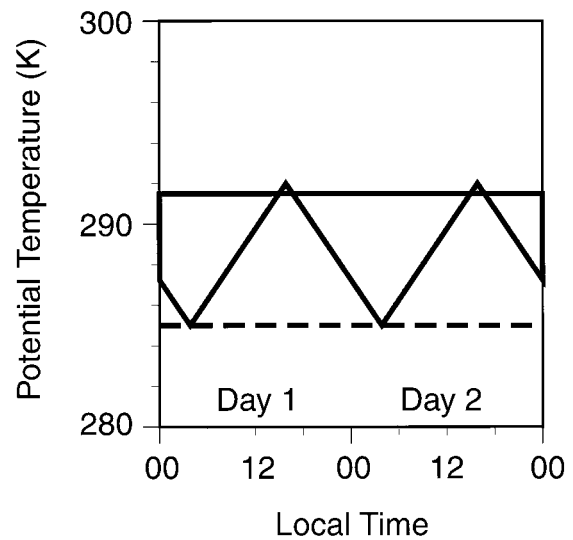


FIG. 9. Simplified pattern of diurnal inversion buildup and destruction as expressed for a sequence of 0400 and 1600 MST soundings. The upper solid line is the basin top potential temperature, the lower solid line is the surface potential temperature, and the dashed line connects the 0400 MST surface potential temperatures.

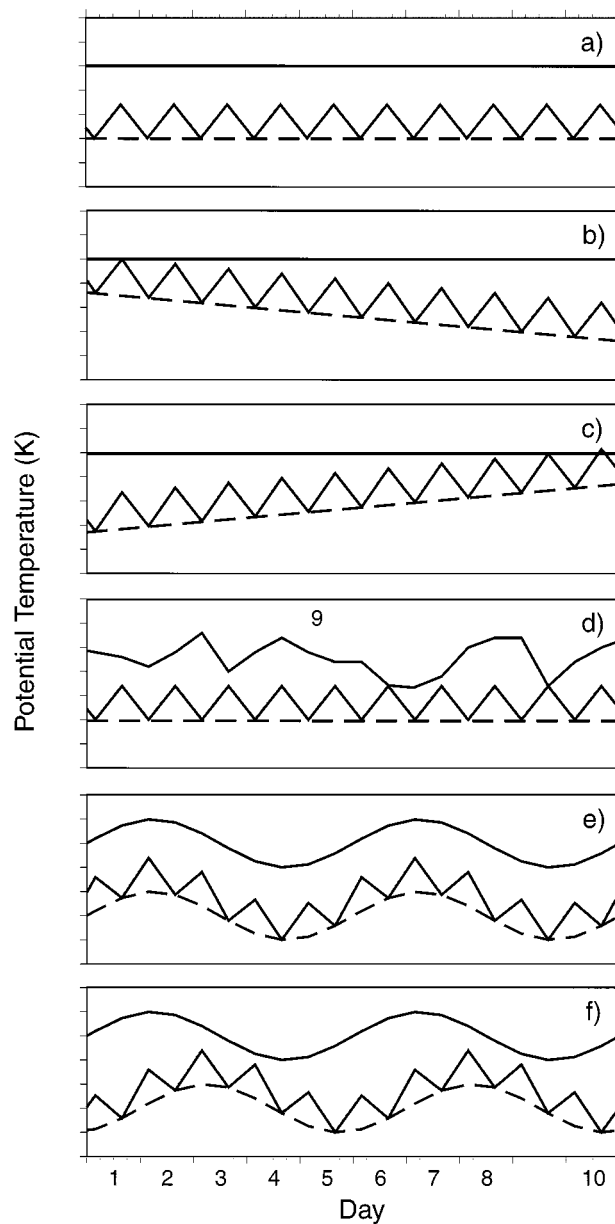


FIG. 10. Simplified evolution patterns for persistent multiday inversions. The upper solid line is the potential temperature at the top of the basin, the lower solid line is the potential temperature on the basin floor, and the dashed line connects the morning potential temperatures at the basin floor. The shading represents the basin potential temperature deficit or inversion. See text for descriptions of (a)–(f).

11–14 and 54–57). Figures 10d–f depict the simplified patterns that result when the basin cold pool is considered to be driven primarily by changes in potential temperature at the top of the basin. Pattern (d) would occur if potential temperature changes above the cold pool were not communicated to the underlying stable layer. In contrast, (e) assumes that potential temperature oscillations aloft are instantly communicated to the underlying cold pool, and (f) assumes that potential tem-

perature oscillations at the ground lag the oscillations aloft. The lag in pattern (f) could occur, for example, if air from above the basin were cooled on the upper slopes of the basin and drained into the basin each night over a series of days. Figure 7 shows that there are times when each of the patterns (d)–(f) play a role in cold pool evolution. Pattern (d) occurs frequently, and there are times when the envelope of surface temperature minimums parallels temperature oscillations at the basin top with varying time lags, as suggested by patterns (e) and (f). The lag times applying to pattern (f), however, are not consistent from episode to episode and the overall pattern of cold pool evolution is more complicated than can be explained by combinations of the simple patterns.

A complication of persistent multiday inversions is that the surface and basin top temperatures can become decoupled over a period of days. See, for example, the temperatures during the period from days 11–15 in Fig. 7 when the surface temperatures rise while the basin top temperatures fall. Temperatures above the basin vary with the synoptic-scale temperature advection associated with traveling weather systems; temperature variations at the basin surface, on the other hand, are driven primarily by smaller-scale processes associated with diurnal boundary layer development inside the basin. Daily destruction of a basin inversion, in contrast to the persistent multiday inversion case, is accompanied by vertical mixing that causes the surface temperatures to equilibrate with temperatures at the basin top every afternoon. This daily recoupling of the basin and above-basin atmospheres allows the envelope of surface minimum temperatures to accurately track (in the absence of clouds or precipitation) long-term oscillations in basin top potential temperature. This feature is clearly seen in Fig. 7 following day 71.

6. Evolution of the atmospheric heat deficit in the basin

In the previous section the evolution of the basin inversion was investigated by considering time series of potential temperature measurements at the basin floor and top. In this section, a more quantitative assessment of inversion evolution is developed by considering heat storage in the basin inversion.

A basin potential temperature inversion is a surface-based layer of potentially cold air or, stated alternately, a surface-based layer in which potential temperature increases with height. The heat Q required to destroy an inversion of depth h is

$$Q = c_p \int_0^h \rho(z) [\theta_h - \theta(z)] A(z) dz \quad [\text{J}], \quad (1)$$

where ρ is air density, c_p is the specific heat of air at constant pressure, $\theta(z)$ is potential temperature within the inversion, θ_h is the potential temperature at the top of the pool, $A(z)$ is the horizontal area of the integration

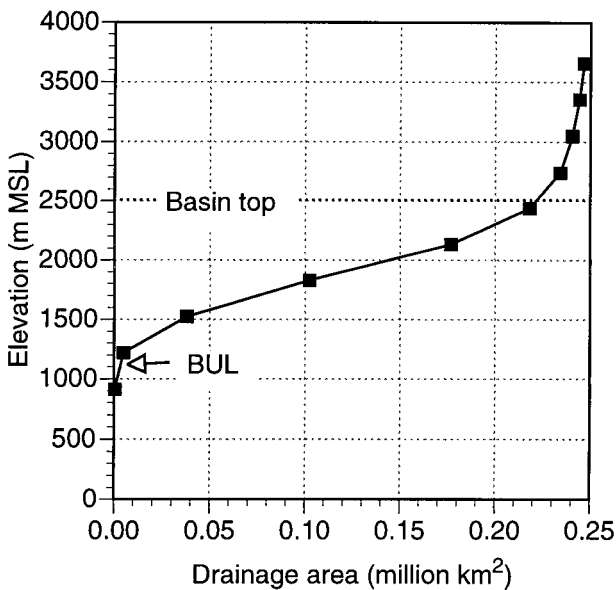


FIG. 11. Horizontal drainage area as a function of altitude for the Colorado Plateau Basin. The altitude of Bullfrog Basin is indicated by an arrow.

volume, and z is height. The *heat deficit* of the pool Q is the heat that must be added to obtain an atmosphere with a height-independent potential temperature θ_h . Temporal changes in the heat deficit calculated at regular intervals in this way provide a means of determining if the basin inversion is building, being maintained, or being destroyed. Division of the heat deficit by the drainage area at the height of the inversion top (223 175 km² in the Colorado Plateau Basin) results in a normalized heat deficit, with units of joules per square meter, representing an equivalent heat flow through the top of the volume and providing a basis for future comparisons of heat flows in basins of differing geometry.

The basin heat deficit was calculated from (1) up to the basin depth (i.e., $h = 1400$ m AGL) over 100-m intervals for an 80-day sequence of Bullfrog Basin twice-daily potential temperature soundings using the basin drainage area versus height relationship $A(z)$ in Fig. 11 derived from a topographic map. The result, when divided by the drainage area at the top of the basin, is plotted in Fig. 12a. Also shown in Fig. 12 are subfigures of basin top, surface, and 70-kPa potential temperatures at Bullfrog Basin (Fig. 12b), 70-kPa geopotential heights at Bullfrog Basin (Fig. 12c), 24-h total precipitation water equivalent at 1500 MST at Tusayan (Fig. 12d), clearness index for Mexican Hat (Fig. 12e), 70-kPa and surface (actually, 10-m AGL) wind speeds at Bullfrog Basin (Fig. 12f), and 70-kPa wind directions at Bullfrog Basin (Fig. 12g). These subfigures are included to examine the timing of inversion buildup and breakup with respect to synoptic and local weather variables. The clearness index is the ratio of measured daily total solar radiation and the theoretically calculated daily

extraterrestrial solar radiation determined by Whiteman and Allwine's (1986) solar model. This ratio is highest (about 0.8) on clear days and lowest on cloudy days; its daily calculated value is plotted at both the 0400 and 1600 observation times. Precipitation during the experimental period fell primarily as snow at the Tusayan site but fell as rain after 12 March. Figures 12a and 12b allow a comparison between the two alternative approaches (potential temperature gradient and normalized heat deficit) for determining basin inversion occurrence and strength.

Inversion buildup is represented in Fig. 12a by a series of rising 12-hourly heat deficit steps, dissipation by descending steps, and complete breakup by a negligible heat deficit. The number and size of the steps required to build or break the inversion gives a graphic illustration of the timescale and strength of the processes involved. Major episodes of buildup, maintenance, and destruction are highlighted by shaded vertical strips in the figure. The width of the strips corresponds to time intervals exceeding 24 h in which the steps remain above an arbitrary threshold of 1.1 MJ m^{-2} . This threshold, marked on the figure by the symbol γ_s , corresponds to the normalized heat deficit that would be produced in the basin if its potential temperature gradient were equivalent to that of the National Advisory Committee for Aeronautics standard atmosphere (0.0033 K m^{-1}). Also shown on the figure, and marked with the symbol γ_i , is the normalized heat deficit corresponding to an isothermal basin atmosphere. The major episodes occur most frequently during midwinter, when they are driven by synoptic-scale events. They decrease in strength and persistence as spring approaches and the daily cycle of heating and cooling begins to play the major role in basin inversion evolution. The daily cycle produces steps with a magnitude near 0.5 MJ m^{-2} that are seen throughout the experimental period, but are especially prominent after day 60. The strength of the daily cycle steps increases from midwinter to spring. A regular day/night oscillation in 70-kPa temperatures after day 78 (Fig. 12b) is an indication that the inversion is being destroyed on a daily basis, since daytime convection clearly reaches the 70-kPa pressure level. The major wintertime episodes of buildup and breakup, however, occur in steps that are much larger than the daily steps and so appear to be influenced primarily by synoptic-scale processes. Nonetheless, all inversion breakups in the 80-day period occurred in the afternoon rather than the morning, and inversion buildups were generally strongest in the morning soundings. This evidence supports the conclusion of Savoie and McKee (1995), for January and February observations in the Great Basin, that radiation-driven heat additions and subtractions play mostly a supporting role in wintertime inversion buildup and breakup. From Fig. 12a, inversion destruction occurs on the afternoons of days 14, 29, 33, 44, 45, 46, 52, 58, 61, 63, and 65 and on a succession of days later in the period. A series of days in which the

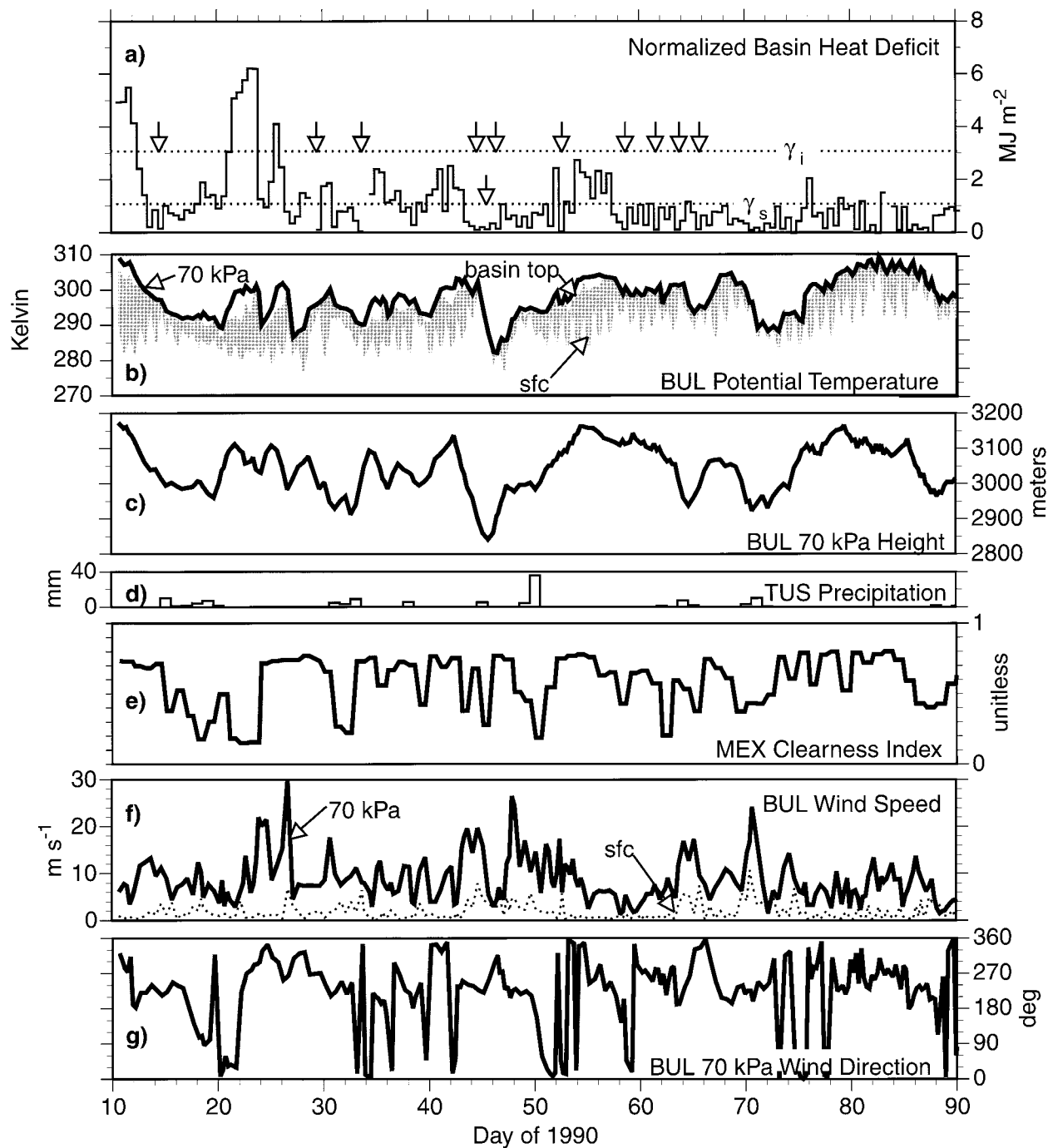


FIG. 12. Times series of Bullfrog Basin data during the experimental period. (a) Heat required to break the basin inversion; (b) 70-kPa, basin top, and surface potential temperatures at BUL; (c) 70-kPa geopotential height at BUL; (d) 24-h precipitation ending at 1500 MST at TUS; (e) clearness index at MEX; (f) 70-kPa and surface wind speeds at BUL; and (g) 70-kPa wind directions at BUL. Major inversion episodes are indicated by shaded vertical strips. Arrows in (a) indicate times of complete inversion destruction. The line labeled with γ_i is the basin heat deficit corresponding to an isothermal atmosphere, while γ_s is the deficit corresponding to a standard atmosphere potential temperature gradient of $\partial\theta/\partial z = 0.0033 \text{ K m}^{-1}$.

normalized basin heat deficit remains above zero are multiday inversion episodes. The longest multiday episode occurs between days 14 and 29.

Figure 12c shows that a series of troughs and ridges

passed through the area during the experimental period. Temperatures at 70 kPa (Fig. 12b) are closely related to the movement of passing synoptic-scale pressure systems because of the tendency for cold air to form in

low pressure troughs and warm air to form in high pressure ridges on the 70-kPa pressure surface. There is thus a good correlation between the 70-kPa height and temperature fields and, in this area of generally westerly winds (see Fig. 12g), warm air advection occurs ahead of approaching ridges and cold air advection occurs in advance of approaching troughs (Figs. 12b, c). High winds (Fig. 12f) tend to occur with trough passages, but there are many exceptions to this rule. Major inversion episodes occur with high pressures and temperatures at the 70-kPa level. Inversions build up in the basin as warm air advection occurs in advance of the approaching ridges and are destroyed as cold air advection occurs ahead of approaching troughs. The destruction of the basin inversion is not assured by the approach of a trough, however, and there are many cases when troughs passed through the experimental area without breaking the basin inversion. These include a deep trough on day 19 and weaker troughs on days 24, 27, 36, 39, 50, and 65.

Basin inversion buildup during major episodes usually takes place over one or more days (Fig. 12a). The warm air advection in major episodes is often initiated when winds aloft develop an easterly component (Fig. 12g). Potential temperatures at 70 kPa rise gradually over a period of days, but warming at the basin top lags the 70-kPa warming by 1–3 days (Fig. 12b). The more rapid warming at 70 kPa than at the basin top stabilizes the atmosphere above the basin. The stabilization of the above-basin atmosphere at the beginning of major buildup periods is an explanation for the lack of sharp changes in stability at the top of the basin. The buildup usually takes place with rising steps that are much larger than the 0.5 MJ m^{-2} diurnal steps, suggesting that buildups are not produced primarily by a series of clear nights in which cold air accumulates in the basin. The buildup is complete when the ridge is overhead and 70-kPa temperatures reach their maximum. The basin inversion (Fig. 12a) can persist for several days while maintaining its strength as long as the high-pressure system and its accompanying warm temperatures aloft are maintained. There are, however, often diurnal modulations in inversion strength during these high persistence episodes. Decay of the inversion inevitably follows as a new trough approaches. Inversion decay generally occurs over shorter time periods than inversion buildup and is accomplished as cold air advection occurs in advance of an approaching trough (Figs. 12b, c). The rapid decays are usually associated with rapid falls of temperature above the basin but are also variously accompanied by rising wind speeds aloft or by increases in cloudiness. Surprisingly, rapid drops of basin heat deficit do not generally lead to complete inversion destruction (complete destruction events before day 70 are indicated by arrows in Fig. 12a). The actual destruction always occurs in the afternoon, usually one or more time steps after the rapid decrease in the heat deficit. This suggests that afternoon convection is necessary to remove the

final inversion remnant. The role of above-basin winds in these final inversion breakup stages is unclear. Some breakups are accompanied by high wind speeds aloft (e.g., day 44), while others occur with relative low speeds aloft (e.g., days 29, 33, 58, 61). There are also instances when high wind speeds aloft are not associated with inversion destruction (e.g., day 24).

Winds at the basin floor (Fig. 12f) are much weaker than winds aloft, exceeding 8 m s^{-1} only after inversion destruction on day 70. The surrounding topography and atmospheric stability apparently are responsible for the protection of the basin floor from the stronger winds aloft. Wind directions at the floor (not shown) vary diurnally, usually blowing toward the north-northeast during daytime and toward the south-southwest during nighttime (see Whiteman et al. 1999b for a description of these winds and their relationship to the regional wind field). Winds at the basin floor increase once the inversion is destroyed. After inversion destruction (or when the basin heat deficit drops below 0.5 MJ m^{-2}) the increased wind speeds at the basin floor can persist for multiday periods (days around 45, 70, and 88).

The relationship between inversion evolution and the clearness index (Fig. 12e), like that between inversion evolution and wind speed aloft, is unclear from the data. Periods with low clearness indices are cloudy periods that sometimes are accompanied by rain or snow (Fig. 12d). When clouds develop above a basin inversion, radiative interactions between the warm cloud and the colder basin floor and sidewalls are expected to destabilize the basin atmosphere, decrease the basin heat deficit, and keep the basin temperatures from falling as low as on clear nights. If the clouds, in contrast, were to form within the basin but near the top of the basin atmosphere, latent heat would be released, increasing stability and the basin heat deficit. The clouds would also have the radiative warming effect for the air below them, however, so that the counteracting or offsetting processes make the final outcome difficult to predict. The data show that low clearness indices are most frequently associated with weak heat deficits during the experimental period but, interestingly, are also found to be associated with the single episode of largest heat deficit on days 20–23.

A comparison (not shown) between Bullfrog Basin and Winslow 70-kPa heights and temperatures shows that these variables are generally well correlated between the two locations and are thus indicative of the larger-scale synoptic flows associated with traveling weather systems that pass through the southwest. Thus, in future work, it should be possible to use the routine twice daily Winslow radiosondes to represent conditions above the Colorado Plateau Basin, at least as far north as Bullfrog Basin. Wind speeds and wind directions at Bullfrog Basin were less well correlated with those at Winslow, but the general trends were similar.

7. Discussion

Temperature inversion buildup and breakup in the Colorado Plateau Basin differ in significant ways from buildup and breakup in smaller valleys and basins. Small valleys (Whiteman 1982, 1990) and basins (Whiteman et al. 1996; Fast et al. 1996) are generally characterized by inversions with distinct tops whose altitudes are found below the surrounding topography. Potential temperature gradients are greater than isothermal in these inversions (mean potential temperature gradients are about 0.025 K m^{-1}), so that temperature increases with height. The winds within inversions in small valleys and basins are relatively isolated from the winds aloft, so long as winds aloft do not become too strong. During clear undisturbed periods, inversion breakup occurs regularly from day to day following patterns of inversion destruction in which the upslope flows remove air from the valley (Whiteman 1990). Compensatory subsidence warms the valley cross section and causes the inversion top to descend during the breakup period. Inversion buildup is also regular from day to day, beginning in the evening as cold air drains down the slopes and converges over the center of the valley or basin, causing a cold air pool to increase in depth and strength through the night (Whiteman 1990). Wintertime observations are available for only a few valleys, but Colorado's Eagle and Yampa Valleys (Whiteman 1982) undergo regular diurnal cycles on undisturbed winter days in which inversion strength, inversion top height, and decoupling from winds aloft follow the general rules mentioned above. In the case of the Yampa Valley, the inversion is not destroyed on a typical winter day, but is built up again the following night as cold air drains off the surrounding mountainsides. In contrast, wintertime inversions in the Colorado Plateau Basin often do not have a distinct high stability top separating the basin from the free atmosphere above. They have relatively weak potential temperature gradients and are more affected by the synoptic flows and their accompanying temperature advections, especially at the upper elevations of the basin. These characteristics suggest that the basin is so wide that the confining topography cannot protect the basin atmosphere adequately from the synoptic-scale influences.

8. Summary and conclusions

The Colorado River drainage upstream from the Grand Canyon has been called the Colorado Plateau. The plateau is surrounded by mountains and frequently traps cold air in winter, so that it has the meteorological characteristics of a large basin. A persistent potential temperature inversion forms in this large ($223\,175 \text{ km}^2$) basin in winter.

The wintertime and early spring buildup, maintenance, and dissipation of the basin inversion were investigated using two differing analytical approaches. In

the first approach, relative changes in potential temperatures at the floor and top of the basin were used to monitor inversion buildup, maintenance, and decay. This approach showed a more or less regular diurnal change in temperature at the basin floor, but large potential temperature oscillations of differing periods at the basin top. The second approach used a basin heat deficit as computed from deviations of potential temperature in the basin relative to the temperature at the basin top, weighted by the basin volume in various altitude intervals. This approach casts the temperature inversion evolution problem in a quantitative energetics framework that takes account of actual basin topography. Heat deficit variations with time are used to determine whether the basin inversion is strengthening or weakening.

During the experimental period, inversions usually extended through the entire 1400-m depth of the basin in the morning, producing a mean potential temperature gradient in the basin of 0.0061 K m^{-1} . Because the inversions frequently extended above the basin, with no sharp differences in stability to mark an inversion top, and because the potential temperature gradients were often less stable than isothermal, the term cold air pool is often an inappropriate descriptor of these basin inversions.

Changes in basin heat deficit in midwinter are caused primarily by synoptic-scale processes rather than by heating or cooling from local-scale processes inside the basin. Inversion buildup in winter usually takes place over multiday periods when warm air advection occurs aloft in advance of approaching synoptic-scale ridges, while inversion decay occurs over shorter time periods as cold air advection occurs above the basin in advance of passing synoptic-scale troughs.

The basin inversion, once formed, can persist for multiday periods because the weak daily heating in wintertime cannot provide the thermal energy necessary to overcome the basin heat deficit. The persistent stable atmosphere in the basin protects the basin somewhat (especially the lowest elevations) from the stronger overlying winds. Thus, winds in the lower elevations of the basin are relatively weak and variable in direction. Inversion strength during these persistence periods is modulated primarily by synoptic-scale warm and cold air advection above the basin, but is also modified diurnally at its base by the daytime growth of a shallow CBL containing upslope flows and the nighttime buildup of a shallow stable sublayer containing downslope flows. These sublayers follow the topography within the basin, forming over both horizontal and inclined slopes. The short daytime heating period during the winter season and the strength of the basin inversion result in CBL growth at the floor of the basin that often reaches only 400–600 m AGL, allowing the elevated remnants of the nocturnal inversion to persist in the upper altitudes of the basin. The CBLs can often break the inversion at higher elevations on the upper sidewalls of the basin,

however. In midwinter, the basin inversion can decay rapidly (often over periods shorter than 12 h) as troughs approach. The decay, however, is often insufficient to completely break the inversion. The final destruction of the inversion, when it does occur, is usually accomplished after the rapid decay period (sometimes more than 24 h later) with help from afternoon convective boundary layers that grow upward from the basin floor. As spring approaches, the basin heat deficit decreases and the more energetic CBLs grow deeper, eventually beginning to break the inversion on a daily basis after the end of February.

This paper has presented the bulk characteristics and long-term evolution of basin inversions. The basin inversions in midwinter exhibited considerable day-to-day variability in strength and depth. The mechanisms leading to inversion buildup and breakup in this large basin appear to be much more complicated than mechanisms for inversion buildup and breakup in smaller valleys and basins, perhaps because the basin atmosphere is not as well protected by surrounding topography from synoptic-scale flow intrusions.

Further observational and modeling studies are needed to determine the detailed mechanisms leading to basin inversion evolution, especially those occurring on timescales shorter than 12 h. These mechanisms could not be adequately evaluated with the data at hand because of the coarse time resolution of the data and the near-instantaneous profiles represented by the ascending radiosonde balloons. This is particularly true for inversion decay and destruction, which can occur very quickly, sometimes between adjacent twice-daily radiosondes. Further data will be necessary, for example, to evaluate the roles of turbulent erosion and cloud radiative destabilization in breakup episodes and to support modeling studies that can quantitatively evaluate different mechanisms. Results from the present study suggest that future studies should be conducted over periods of at least several months because of the need to sample seasonal changes in the relative roles of synoptic- and local-scale mechanisms. They must also sample the wind and temperature structure on short time intervals (e.g., hourly) and have good vertical resolution at altitudes near the basin top. Continuously operating, remote sensing, profiling systems seem well suited for such studies, but the present capabilities for remote sounding of vertical temperature structure may not have sufficient range for basins as deep as the Colorado Plateau Basin. Future simulations with dynamical meteorological models may prove useful in investigating both short-term (<24 h) and long-term buildup and breakup mechanisms.

Acknowledgments. Chris Doran, Matt Savoie, and Vic Morris assisted with data collection at Buffalo Ranch. Jerry Allwine and Matt Savoie assisted in data processing. Stephan de Wekker provided useful comments on an early version of the manuscript. Paul Ostapuk's

comments on the same manuscript provided a much-appreciated weather forecasting perspective. Research was supported by Arizona's Salt River Project (project manager, Prem Bhardwaja) under Contract VN-08005-CAS with Battelle's Pacific Northwest Laboratories and by the U.S. Department of Energy's Environmental Sciences Division as part of their Atmospheric Studies in Complex Terrain program under Contract DE-AC06-76RLO 1830 at Pacific Northwest National Laboratory. Pacific Northwest National Laboratory is operated by Battelle Memorial Institute for the U.S. Department of Energy.

REFERENCES

- Allwine, K. J., and C. D. Whiteman, 1994: Single-station integral measures of atmospheric stagnation, recirculation and ventilation. *Atmos. Environ.*, **28**, 713–721.
- , B. K. Lamb, and R. Eskridge, 1992: Wintertime dispersion in a mountainous basin at Roanoke, Virginia: Tracer study. *J. Appl. Meteor.*, **31**, 1295–1311.
- Banta, R. M., 1984: Daytime boundary layer evolution over mountainous terrain. Part I: Observations of the dry circulations. *Mon. Wea. Rev.*, **112**, 340–356.
- , L. S. Darby, P. Kaufmann, D. H. Levinson, and C.-J. Zhu, 1999: Wind-flow patterns in the Grand Canyon as revealed by Doppler lidar. *J. Appl. Meteor.*, **38**, 1069–1083.
- Chen, J., and Coauthors, 1999: Transport of a power plant tracer plume over Grand Canyon National Park. *J. Appl. Meteor.*, **38**, 1049–1068.
- Doran, J. C., and S. Zhong, 1994: Regional drainage flows in the Pacific Northwest. *Mon. Wea. Rev.*, **122**, 1158–1167.
- Fast, J. D., S. Zhong, and C. D. Whiteman, 1996: Boundary layer evolution within a canyonland basin. Part II: Numerical simulations of nocturnal flows and heat budgets. *J. Appl. Meteor.*, **35**, 2162–2178.
- Glendening, J. W., 1990: A mixed-layer simulation of daytime boundary layer variations within the Los Angeles Basin. *Mon. Wea. Rev.*, **118**, 1531–1550.
- Harris, D. V., 1978: *The Geologic Story of the National Parks and Monuments*. Colorado State University Foundation Press, 325 pp.
- Holzworth, G. C., 1972: Mixing heights, wind speeds and potential for urban air pollution throughout the contiguous United States. Office of Air Programs Publ. AP-101, U.S. Environmental Protection Agency, 118 pp.
- , and R. W. Fisher, 1979: Climatological summaries of the lower few kilometers of rawinsonde observations. EPA-600/4-79-026, U.S. EPA, 141 pp.
- Ishikawa, N., 1977: Studies of radiative cooling at land basins in snowy season. *Contrib. Inst. Low Temp. Sci.*, **27A**, 1–46.
- Kaufmann, P., and C. D. Whiteman, 1999: Cluster-analysis classification of wintertime wind patterns in the Grand Canyon region. *J. Appl. Meteor.*, **38**, 1131–1147.
- Kimura, F., and T. Kuwagata, 1993: Thermally induced wind passing from plain to basin over a mountain range. *J. Appl. Meteor.*, **32**, 1538–1547.
- Kondo, J., and N. Okusa, 1990: A simple numerical prediction model of nocturnal cooling in a basin with various topographic parameters. *J. Appl. Meteor.*, **29**, 604–619.
- , T. Kuwagata, and S. Haginoya, 1989: Heat budget analysis of nocturnal cooling and daytime heating in a basin. *J. Atmos. Sci.*, **46**, 2917–2933.
- Kuwagata, T., and M. Sumioka, 1991: The daytime PBL heating process over complex terrain in central Japan under fair and calm weather conditions. Part III: Daytime thermal low and nocturnal thermal high. *J. Meteor. Soc. Japan*, **69**, 91–104.

- , N. Masuko, M. Sumioka, and J. Kondo, 1990a: The daytime PBL heating process over complex terrain in central Japan under fair and calm weather conditions. Part II: Regional heat budget, convective boundary layer height and surface moisture availability. *J. Meteor. Soc. Japan*, **68**, 639–650.
- , M. Sumioka, N. Masuko, and J. Kondo, 1990b: The daytime PBL heating process over complex terrain in central Japan under fair and calm weather conditions. Part I: Meso-scale circulation and the PBL heating rate. *J. Meteor. Soc. Japan*, **68**, 625–638.
- Lindsey, C. G., J. Chen, T. S. Dye, L. W. Richards, and D. L. Blumenthal, 1999: Meteorological processes affecting the transport of emissions from the Navajo Generating Station to Grand Canyon National Park. *J. Appl. Meteor.*, **38**, 1031–1048.
- Lu, R., and R. P. Turco, 1995: Air pollutant transport in a coastal environment—II. Three-dimensional simulations over Los Angeles Basin. *Atmos. Environ.*, **29**, 1499–1518.
- , and —, 1996: Ozone distributions over the Los Angeles Basin: Three-dimensional simulations with the SMOG model. *Atmos. Environ.*, **30**, 4155–4176.
- Mayr, G. J., and T. B. McKee, 1995: Observations of the evolution of orogenic blocking. *Mon. Wea. Rev.*, **123**, 1447–1464.
- Panofsky, H. A., and G. W. Brier, 1965: *Some Applications of Statistics to Meteorology*. The Pennsylvania State University, 224 pp.
- Petkovsek, Z., 1974: Dissipation of the upper layer of all-day radiation fog in basins. *Zb. Meteor. Hidrol. Rad.*, **5**, 71–74.
- , 1978: Relief meteorologically relevant characteristics of basins. *Z. Meteor.*, **28**, 333–340.
- , 1980: Additional relief meteorologically relevant characteristics of basins. *Z. Meteor.*, **30**, 379–382.
- , 1992: Turbulent dissipation of cold air lake in a basin. *Meteor. Atmos. Phys.*, **47**, 237–245.
- Reddy, P. J., D. E. Barbarick, and R. D. Osterburg, 1995: Development of a statistical model for forecasting episodes of visibility degradation in the Denver metropolitan area. *J. Appl. Meteor.*, **34**, 616–625.
- Richards, L. W., C. L. Blanchard, and D. L. Blumenthal, Eds., 1991: Navajo Generating Station visibility final report. Rep. STI-90200-1124-FR, Sonoma Technology, Inc., Santa Rosa, CA, 408 pp. [Available from Salt River Project, P.O. Box 52025, Phoenix, AZ 85072-2025.]
- Savoie, M. H., and T. B. McKee, 1995: The role of wintertime radiation in maintaining and destroying stable layers. *Theor. Appl. Climatol.*, **52**, 43–54.
- Smith, R., and Coauthors, 1997: Local and remote effects of mountains on weather: Research needs and opportunities. *Bull. Amer. Meteor. Soc.*, **78**, 877–892.
- Smith, T. B., D. L. Blumenthal, and S. L. Marsh, 1980: Summary of meteorology in the Los Angeles Basin during ACHEX I and II. *The Character and Origins of Smog Aerosols: A Digest of Results from the California Aerosol Characterization Experiment (ACH-EX)*. G. M. Hidy et al., Eds., Advances in Environmental Sciences and Technology, Vol. 9, John Wiley and Sons, 585–591.
- Staley, D. O., 1959: Some observations of surface-wind oscillations in a heated basin. *J. Meteor.*, **16**, 364–370.
- Sutherland, J. L., 1992: Surface wind observations in the region of the Grand Canyon and Lake Powell. Preprints, *Sixth Conf. on Mountain Meteorology*, Portland, OR, Amer. Meteor. Soc., 151–155.
- Ulricksen, B. L., and C. F. Mass, 1990: Numerical investigations of mesoscale circulations over the Los Angeles Basin. Part II: Synoptic influences and pollutant transport. *Mon. Wea. Rev.*, **118**, 2162–2184.
- Vrhovec, T., 1991: A cold air lake formation in a basin—A simulation with a mesoscale numerical model. *Meteor. Atmos. Phys.*, **46**, 91–99.
- Whiteman, C. D., 1982: Breakup of temperature inversions in deep mountain valleys: Part I. Observations. *J. Appl. Meteor.*, **21**, 270–289.
- , 1990: Observations of thermally developed wind systems in mountainous terrain. *Atmospheric Processes over Complex Terrain*, *Meteor. Monogr.*, No. 45, Amer. Meteor. Soc., 5–42.
- , and K. J. Allwine, 1986: Extraterrestrial solar radiation on inclined surfaces. *Environ. Software*, **1**, 164–169.
- , T. B. McKee, and J. C. Doran, 1996: Boundary layer evolution within a canyonland basin. Part I: Mass, heat, and moisture budgets from observations. *J. Appl. Meteor.*, **35**, 2145–2161.
- , S. Zhong, and X. Bian, 1999a: Wintertime boundary layer structure in the Grand Canyon. *J. Appl. Meteor.*, **38**, 1084–1102.
- , X. Bian, and J. L. Sutherland, 1999b: Wintertime surface wind patterns in the Colorado River Valley. *J. Appl. Meteor.*, **38**, 1118–1130.
- Wolyn, P. G., and T. B. McKee, 1989: Deep stable layers in the intermountain Western United States. *Mon. Wea. Rev.*, **117**, 461–472.